Purdue University

Purdue e-Pubs

Faculty Publications

Department of Computer Information Technology

5-27-2020

A Statistical Impulse Response Model Based on Empirical Characterization of Wireless Underground Channel

Abdul Salam
Purdue University, salama@purdue.edu

Mehmet C. Vuran

Suat Irmak

Follow this and additional works at: https://docs.lib.purdue.edu/cit_articles

Part of the Digital Communications and Networking Commons, OS and Networks Commons, Other Earth Sciences Commons, Soil Science Commons, Sustainability Commons, Systems and Communications Commons, and the Systems Architecture Commons

A Statistical Impulse Response Model Based on Empirical Characterization of Wireless Underground Channel

Abdul Salam, *Member, IEEE,* Mehmet C. Vuran, *Member, IEEE*,

and Suat Irmak

Abstract

Wireless underground sensor networks (WUSNs) are becoming ubiquitous in many areas. The design of robust systems requires extensive understanding of the underground (UG) channel characteristics. In this paper, an UG channel impulse response is modeled and validated via extensive experiments in indoor and field testbed settings. The three distinct types of soils are selected with sand and clay contents ranging from 13% to 86% and 3% to 32%, respectively. The impacts of changes in soil texture and soil moisture are investigated with more than $1,200$ measurements in a novel UG testbed that allows flexibility in soil moisture control. Moreover, the time-domain characteristics of the channel such as the the RMS delay spread, coherence bandwidth, and multipath power gain are analyzed. The analysis of the power delay profile validates the three main components of the UG channel: direct, reflected, and lateral waves. Furthermore, it is shown that the RMS delay spread follows a log-normal distribution. The coherence bandwidth ranges between $650\,\mathrm{kHz}$ and $1.15\,\mathrm{MHz}$ for soil paths of up to $1\,\mathrm{m}$ and decreases

A. Salam is with the Department of Computer and Information Technology, Purdue University, West Lafayette, IN (e-mail: salama@purdue.edu).

M. C. Vuran is with the Department of Computer Science and Engineering, University of Nebraska-Lincoln, Lincoln, NE (e-mail: mcvuran@cse.unl.edu).

Suat Irmak is with Department of Biological Systems Engineering, University of Nebraska-Lincoln, Lincoln, NE 68583 Email: sirmak2@unl.edu.

to $418\,\text{kHz}$ for distances above $10\,\text{m}$. Soil moisture is shown to affect the RMS delay spread non-linearly, which provides opportunities for soil moisture-based dynamic adaptation techniques. Based on the measurements and the analysis, a statistical channel model for wireless underground channel has been developed. The statistical model shows good agreement with the measurement data. The model and analysis paves the way for tailored solutions for data harvesting, UG sub-carrier communication, and UG beamforming.

Index Terms

Cyber-physical systems, Underground electromagnetic propagation, Wireless underground sensor networks, Precision agriculture.

I. INTRODUCTION

WIRELESS underground sensor networks (WUSNs) are becoming ubiquitous in many areas including precision agriculture [1], [2], [12], [29], [42], [48], [56], [57], [58], [60], [74], environment and infrastructure monitoring [14], [20], [68], [71], [3], and border patrol [5]. The establishment of robust wireless underground communication links between two underground nodes (UG2UG links) or an underground node and a node above the surface (UG2AG links) requires extensive knowledge of the underground (UG) channel characteristics.

In general, the performance of a communication system is seriously degraded by multipath fading [15]. Moreover, the communication in UG channel is affected by multipath fading caused by reflection of electromagnetic (EM) waves in soil and from soil-air interface. Tp reduce the effects of these disturbances, a detailed characterization of the UG channel is required. Traditional over-the-air (OTA) communication channel models cannot be readily used in WUSNs because EM waves in soil suffer higher attenuation than in air due to their incidence in lossy media which consists of soil, water and air, and accordingly, leads to permittivity variations over time and space with changes in soil moisture [12]. The WUSNs are generally deployed at depths which are less than $50\,\text{cm}$ [8]. Due to proximity to the Earth surface, a part of the transmitted EM waves propagate from soil to air, then travel along the soil-air interface, and enter the soil again to reach the receiver. These EM waves (*lateral waves* [18]) are a major component of the UG channel.

The analysis of EM wave propagation in underground channel is challenging because of its computation complexity [5]. In [11] and [73], channel models based on the analysis of the EM field and Friis equations have been developed and direct, reflected, and lateral waves are shown

to be major contributors of received signal strength. These models provide good approximations when coarse channel measures (e.g., path loss) are concerned but are limited due to the lack of insight into channel statistics (e.g., delay spread, and coherence bandwidth) and empirical validations.

Partly unique to the UG channel, there are mainly four types of physical mechanisms that lead to variations in the UG channel statistics, the analyses of which constitute the major contributions of this paper.

1) Soil Texture and Bulk Density Variations: EM waves exhibit attenuation when incident in soil medium. These variations vary with texture and bulk density of soil. For example, sandy soil holds less bound water, which is the major component in soil that absorbs EM waves. The water holding capacity of medium textured soils (silt loam, fine sandy loam, and silty clay loam) is much higher, because of the small pore size, as compared to coarse soils (sand, sandy loam, loamy sand). Medium textured soils have lower pore size and hence, no aggregation and little resistance against gravity [13]. To cover a wide array of soil texture and bulk density variations, we have performed experiments in three distinct types of soils.

2) Soil Moisture Variations: The effective permittivity of soil is a complex number, thus, besides diffusion attenuation, the EM waves also suffer from an additional attenuation caused by the absorption of soil water content. To this end, experiments are conducted with controlled soil moisture variations in an indoor testbed.

3) Distance and Depth Variations: Received signal strength varies with depth of and distance between transmitter and receiver antennas because different components of EM waves suffer attenuation based on their travel paths. Sensors in WUSN applications are usually buried in topsoil and subsoil layers. The topsoil layer (root growth region) consists of top $1\,\mathrm{feet}$ of soil and $2-4\,\mathrm{feet}$ layer below the topsoil is subsoil. Therefore, we have taken measurements for depths of $10-40\,\mathrm{cm}$ with transmitter receiver (T-R) distances of $50\,\mathrm{cm}$ to $12\,\mathrm{m}$ for UG2UG experiments. Near-field effects of underground antenna for frequency range used in these experiments are within the $30\,\mathrm{cm}$ region. In addition, UG2AG experiments are conducted for radii of $2-7\,\mathrm{m}$ with receiver angles of 0°-90° taken in the vertical plane as normal to soil-air interface.

4) Frequency Variations: The path loss caused by the attenuation is frequency dependent [10]. In addition, when EM waves propagate in soil, their wavelength shortens due to higher permittivity of soil than the air. Channel capacity in soil is also a function of operation frequency. Channel transfer function measurements (S_{21}) are taken to analyze the effects of frequency on

underground communication [63], [28], [65], [59], [61], [75], [74], [19], [55], [57], [31], [54], [56], [39], [32], [34], [37], [52], [38], [70], [36], [33], [42], [51], [35], [43], [40], [48], [47], [44], [49], [45], [46], [50], [41], [25], [26], [53], [24], [27].

Given the effects of these factors, the optimization of digital communications in wireless underground channel merits a detailed characterization of effects of these physical phenomena of soil on propagation between wireless underground channel transmitter and receiver. This requires extensive measurements to derive the model channel parameters such as the RMS delay spread, channel gains, and coherence bandwidth, through empirical measurements. These parameters are useful for performance evaluation of a digital communication system operating in wireless underground channel. Therefore, it is important to have a realistic underground channel model. A statistical model developed from empirical observations should not only be able to capture the effects of all the physical processes undergoing in soil but also should exhibit a close match with the measurement data. In this paper, we present an UG channel impulse response model and the corresponding analysis based on measured data collected from UG channel experiments with a $250\,\mathrm{ps}$ delay resolution. Statistical properties of multipath profiles measured in different soil types under different soil moisture levels are investigated. The results presented here describe Root mean square (RMS) delay spread, distribution of the RMS delay spread, mean amplitude across all profiles for a fixed T-R displacement, effects of soil moisture on peak amplitudes of power delay profiles, mean access delay, and coherence bandwidth statistics. The goal of the measurement campaign and the corresponding model is to produce a reliable channel model which can be used for different types of soils under different conditions. Thus, we have considered several possible scenarios with more than $1,500$ measurements taken over a period of 10 months.

The rest of the paper is organized as follows: The related work is discussed in Section III. A description of UG channel impulse response model is given in Section IV. In Section V, measurement sites and procedures are described. The results and analysis of measured impulse responses are presented in Section VI. The wireless underground channel statistical model is presented in Section VII. Finally, the paper is concluded in Section IX.

II. BACKGROUND

Electromagnetic (EM) wave communication in the underground channel consists of three types of links [8], namely underground to aboveground (UG2AG), aboveground to underground (AG2UG), and underground to underground (UG2UG). The soil medium is involved in com-

munication through these three links. Wavelength of an EM wave incident into soil is affected by dielectric properties of the soil. Soil texture and its water holding capacity, bulk density, and salinity affects the propagation of waves. To understand the propagation of waves in soil, it is important to understand the physical processes in soil. Soil medium consists of soil particles, pore space, and water content. Soil particles are divided into silt, sand and clay based on their size. Soils are classified based on the distribution of these particle sizes. The complex dielectric constant of soil consists of ϵ'_s and ϵ''_s. The dielectric constant of a soil that is fully dried is not dependent on frequency can be determined from [72]

$$\epsilon'_s = [1 + 0.44\rho_b]^2, \tag{1}$$

where ρ_b is the bulk density of soil. The bulk density is defined as the ratio of the dry soil mass to bulk soil volume including pore space. The dielectric spectra of the soil becomes more complicated with the increase in moisture content. Water content inside the soil is divided into two: bound and free water. Bound water refers to water held by soil particles in the top layers of soil, and depends on particles surface area which is defined by the soil composition. Water content in the soil can be ascertained by either volumetric or gravimetric bases.

Electromagnetic waves traveling in the soil interact with soil particles, air, free and bound water. The free and bound water molecules, when in interaction electromagnetic waves, exhibit different dielectric dispersion characteristics. Thus, the dielectric constant depends on the frequency of EM waves. While it is called "constant", the dielectric is actually not a constant value in the soil and it changes with several factors, including soil water content. However, in general, the increase in dielectric constant of the soil with water content does not differ greatly with soil type (particle size distribution) particularly in the high-frequency applications. That is why, the dielectric constant is an effective indicator of soil water content in different soil types. In addition to the water content and frequency, other factors such as bulk density and soil texture also effect the permittivity of soil.

In [10], a model of dielectric properties of soil has been proposed for frequencies higher than $1.4\,\mathrm{MHz}$. In [21], Peplinski et.al. has modified the model through extensive measurements to characterize the dielectric behavior of the soil in the frequency range of $300\,\mathrm{MHz}$ to $1.3\,\mathrm{GHz}$. It is given as

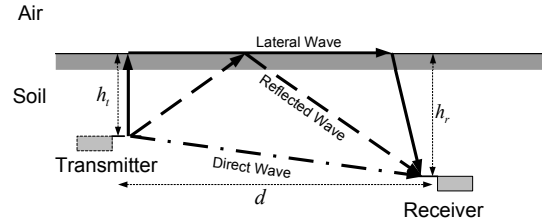$$\epsilon_s = \epsilon'_s - i\epsilon''_s\,, \tag{2}$$

Fig. 1: The three EM waves in an underground channel [11].

where ϵ_s is the relative complex dielectric constant of the soil-water mixture, and it depends on the soil texture, volumetric water content, bulk density, frequency, and particle density.

III. RELATED WORK

Wireless communication in WUSNs is an emerging field and few models exist to represent the underground communication. In [73], we have developed a 2-wave model but lateral wave is not considered. In [7], models have been developed but these do not consider underground communication. A model for underground communication in mines and road tunnels has been developed in [68] but it cannot be applied to WUSN due to wave propagation differences between tunnels and soil. We have also developed a closed-form path loss model using lateral waves in [11] but channel impulse response and statistics cannot be captured through this simplified model.

Wireless underground communication shares characteristics of underwater communication [6]. However, underwater communication based on electromagnetic waves is not feasible because of high attenuation. Therefore, the alternative techniques including acoustic [6] are used in underwater communications. Acoustic technique cannot be used in UG channel due to vibration limitation. In magnetic induction (MI), [20], [69], the signal strength decays with inverse cube factor and high data rates are not possible. Moreover, communication cannot take place if sender receiver coils are perpendicular to each other. Therefore, the MI cannot be readily implemented in WUSNs.

To the best of our knowledge, this is the first measurement campaign conducted to analyze and measure the channel impulse response of UG channel and the first work that proposes guidelines for the development of a novel WUSN testbed to improve the accuracy, to reduce the time required to conduct WUSN experiments, and to allow flexibility in soil moisture control.
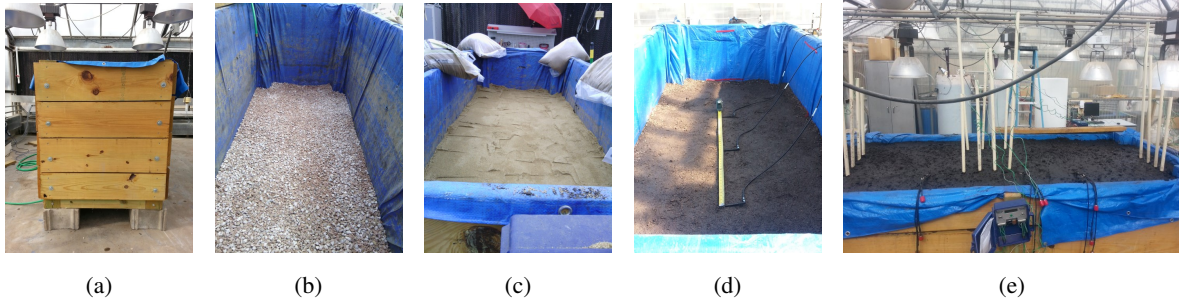
Fig. 2: Testbed Development: (a) Testbed box, (c) Packed soil, (b) Layer of gravel at the bottom of the testbed, (d) Antenna placement, (e) Final outlook.

IV. IMPULSE RESPONSE OF UG CHANNEL

A wireless channel can be completely characterized by its impulse response. Traditionally, a wireless channel is modeled as a linear filter with a complex valued low pass equivalent impulse response which can be expressed as [17]

$$\mathrm{h}(t) = \sum_{l=0}^{L-1} \alpha_l \delta(t - \tau_l) \,, \tag{3}$$

where L is the number of multipaths, α_l are the complex gains, and τ_l the delays associated with multipaths.

A schematic view of UG channel is shown in Fig. 1, where a transmitter and a receiver are located at a distance of d and depths of B_t and B_r, respectively [11]. Communication is mainly conducted through three EM waves. First, the direct wave which travels through the soil in line-of-sight from transmitter to receiver. Second, the reflected wave, that also travels through the soil, is reflected from the air-soil interface. Third, the lateral wave propagates out of soil, travels along the surface and enters the soil to reach the receiver.

Based on this analysis, the UG channel process can be expressed as a sum of direct, reflected and lateral waves. Hence (3) is rewritten for UG channel as

$$\mathrm{h_{ug}}(t) = \sum_{i=0}^{L-1} \alpha_{\mathrm{l},i} \delta(t - \tau_{\mathrm{l},i}) + \sum_{i=0}^{D-1} \alpha_{\mathrm{d},i} \delta(t - \tau_{\mathrm{d},i}) + \sum_{i=0}^{R-1} \alpha_{\mathrm{r},i} \delta(t - \tau_{\mathrm{r},i}) \,, \tag{4}$$

where L, D, and R are number of multipaths; $\alpha_{\mathrm{l},i}$, $\alpha_{\mathrm{d},i}$, and $\alpha_{\mathrm{r},i}$ are the complex gains of a particular wave type with index i; and $\tau_{\mathrm{l},i}$, $\tau_{\mathrm{d},i}$, and $\tau_{\mathrm{r},i}$ are delays associated with lateral wave, direct wave, and reflected wave with index i, respectively.

The received power is the area under the profile and is calculated as the sum of powers in all three components in the profile. Accordingly, the received power is given as

$$P_r = \sum_{i=0}^{L-1} |\alpha_{l,i}|^2 + \sum_{i=0}^{D-1} |\alpha_{d,i}|^2 + \sum_{i=0}^{R-1} |\alpha_{r,i}|^2 \; . \tag{5}$$

The path loss is calculated from the difference of the known transmit power and P_r, and is given as

$$PL(\mathrm{dBm}) = P_t(\mathrm{dBm}) + G_t(\mathrm{dBi}) + G_r(\mathrm{dBi}) - P_r(\mathrm{dBm}) \; , \tag{6}$$

where P_t is transmit power, P_r is received power, and G_t and G_r are transmitter and receiver antenna gains, respectively. The antenna effects are included, intrinsically, in the impulse response $h_{\mathrm{ug}}(t)$ obtained from the channel transfer function. Traditionally, impulse response of wireless indoor channel is also dependent on antenna properties as power radiated and received in a particular direction is defined by directive gains of transmitter and receiver antennas [23]. In our experiments and analysis, we use omni-directional dipole antennas to observe multipath components in all directions.

Next, we review the metrics derived from the channel impulse response, including excess delay and delay spread. Excess delay is the time delay between the first and last arriving components. Last component is defined by a threshold value in dB relative to the strongest component in the power delay profile (PDP). Typically, a threshold value of $-30\,\mathrm{dB}$ is used [15],[23]. Mean excess delay (τ) is defined as the first moment of power delay profile and is given as [23]

$$\tau = \sum_k P_k \tau_k \bigg/ \sum_k P_k \; , \tag{7}$$

where P_k is the absolute instantaneous power at the kth bin, and τ_k is the delay of the kth bin.

Root mean square (RMS) delay spread is the square root of the second central moment of the power delay profile and is given as [23]:

$$\tau_{\mathrm{rms}} = \sqrt{\overline{\tau^2} - (\overline{\tau})^2} \; , \tag{8}$$

where $\overline{\tau^2} = \sum_k P_k \tau_k^2 / \sum_k P_k^2$, P_k is the absolute instantaneous power at k^{th} bin, and τ_k is the delay of the kth bin. The RMS delay spread is a good indicator of multipath spread and it indicates the potential of inter-symbol interference (ISI).
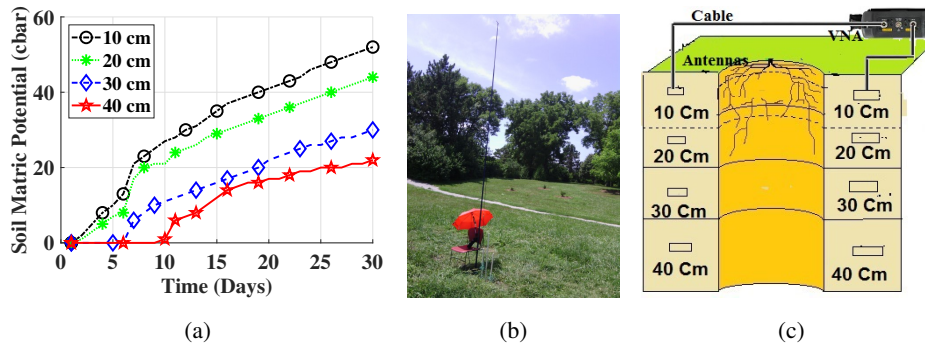
Fig. 3: (a) Soil moisture (expressed as soil matric potential; greater matric potential values indicate lower soil moisture and zero matric potential represents near saturation condition) with time in silt loam testbed, (b) Outdoor testbed in a field setting, (c) Experiment layout.

TABLE I: Particle Size Distribution and Classification of Testbed Soils.

Textural Class	%Sand	%Silt	%Clay
Sandy Soil	86	11	3
Silt Loam	33	51	16
Silty Clay Loam	13	55	32

V. MEASUREMENT SITES AND PROCEDURES

Measurements are conducted in an indoor testbed (Section V-A) and field settings (Section V-B). The measurement procedures are explained in Section V-C.

A. Indoor Testbed

Conducting WUSN experiments in outdoor settings is a challenging task. These challenges include lack of availability of wide range of soil moisture levels over a short period of time, difficulty of dynamic control over soil moisture, changing soil types, and installation/replacement of equipment. Furthermore, extreme temperature affects make it hard to conduct experiments.

To overcome these challenges faced in outdoor environments, an indoor testbed is developed in a greenhouse setting. It is a $100"x36"x48"$ wooden box (Fig. 2(a)) assembled with wooden planks and contains $90\,\mathrm{ft}^3$ of packed soil. A drainage system is installed in the bottom, and sides of the box are covered with water proof tarp to stop water seepage from sides. Before installation of antennas and sensors, $3"$ layer of gravel is laid in the bottom of the box for free drainage of water (Fig. 2(b)) and then soil is placed in the box (Fig. 2(c)). Two pvc drainage outlets installed at the bottom of the testbed allowed freely-drained (due to gravitational force

only) water to exit the system. The soil profile was wetted uniformly in the entire testbed using drip lateral with drip emitters installed every $25\,\mathrm{cm}$ to ensure uniform wetting of the soil profile.

To monitor the soil moisture level, 8 Watermark sensors are installed on each side of the box at $10\,\mathrm{cm}$, $20\,\mathrm{cm}$, $30\,\mathrm{cm}$ and $40\,\mathrm{cm}$ depths. Although in agricultural operations, environmental monitoring and security applications, the soil moisture sensors can be installed at different depths, depending on several variables, most common maximum installation/application depth is about $3\,\mathrm{feet}$ from the soil surface. Depending on the purpose of the soil moisture data use, in many applications such as in shallow-rooted cropping systems, sandy soils and numerous other applications, monitoring soil moisture in the upper soil layer (i.e., $0-40\,\mathrm{cm}$) is sufficient.

These sensors are connected to two Watermark dataloggers. Soil is packed after every $30\,\mathrm{cm}$ by using a tamper tool to achieve the bulk density to mimic real-world field conditions. This process is repeated for antenna installation at each depth. Three sets of four dipole antennas are installed (Fig. 2(d)) at the depths of $10\,\mathrm{cm}$, $20\,\mathrm{cm}$, $30\,\mathrm{cm}$, and $40\,\mathrm{cm}$. These sets are $50\,\mathrm{cm}$ apart from each other. The final outlook of the testbed is shown in Fig. 2(e).

We have conducted experiments for two different types of soils in the indoor testbed: silt loam and sandy soil. Particle size distribution and classification of testbed soils is given in Table I. To investigate the effects of soil texture on underground communication, soils selected for use in the testbed have sand contents ranging from $13\,\%$ to $86\,\%$ and clay contents ranging from $3\,\%$ to $32\,\%$. Before starting the experiments, soil is nearly saturated to attain the highest possible level of volumetric water content (VWC) and then measurements are collected as the water content first reaches to field capacity[1] and then subsequently to wilting point[2]. The changes in soil moisture level with time are shown in Fig. 3(a) for silt loam soil.

B. Field Site

To compare with the results of indoor testbed experiments and conduct underground-to-aboveground experiments, a testbed of dipole antennas has been prepared in an outdoor field with silty clay loam soil (Fig. 3(b)). Dipole antennas are buried in soil at a burial depth of $20\,\mathrm{cm}$ with distances from the first antenna as $50\,\mathrm{cm}$-$12\,\mathrm{m}$. A pole with adjustable height is used to

---

[1]The amount of soil-water held by soil particles after excess water is freely drained, which takes about $2-3\,\mathrm{days}$.

[2]The water content level at which water is no more available to plants.

(a)   (b)

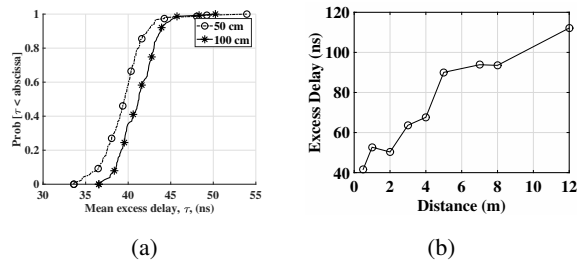Fig. 4: (a) Distribution of mean excess delay τ in indoor testbed (silt loam) experiment, (b) Excess delay with distance at $20\,\mathrm{cm}$ depth in field (silty clay loam) experiment.

conduct underground-to-aboveground (UG2AG) experiments with radii of $2\,\mathrm{m}$, $4\,\mathrm{m}$, $5.5\,\mathrm{m}$ and $7\,\mathrm{m}^3$ with receiver angles of $0°$, $30°$, $45°$, $60°$, and $90°$.

C. Measurement Procedure

Accurate measurement of channel impulse response can be obtained from frequency domain measurements due to Fourier transform relationship between transfer function and channel impulse response [16]. Accordingly, we have obtained channel impulse by taking frequency domain measurements and then taking inverse Fourier transform. A diagram of the measurement layout is shown in Fig. 3(c). Frequency response of the channel is measured using a Vector Network Analyzer (VNA). VNA-based channel measurements are popular for measuring channel transfer functions in wireless communications and antenna domains [9], [15], [16], [23], [66], [67]. The measurement parameters are given in Table II. The VNA generates a linearly swept frequency signal [22] which is propagated over a frequency range of $10\,\mathrm{MHz}$ to $4\,\mathrm{GHz}$. In this

---

[3]The maximum distance of $7\,\mathrm{m}$ is due to the limitations of the antenna cable length for VNA.

TABLE II: Underground channel measurement parameters

Parameter	Value
Start Frequency	$10\,\mathrm{MHz}$
Stop Frequency	$4\,\mathrm{GHz}$
Number of Frequency Points	401
Transmit Power	$5\,\mathrm{dBm}$
Vector Network Analyzer	Agilent FieldFox

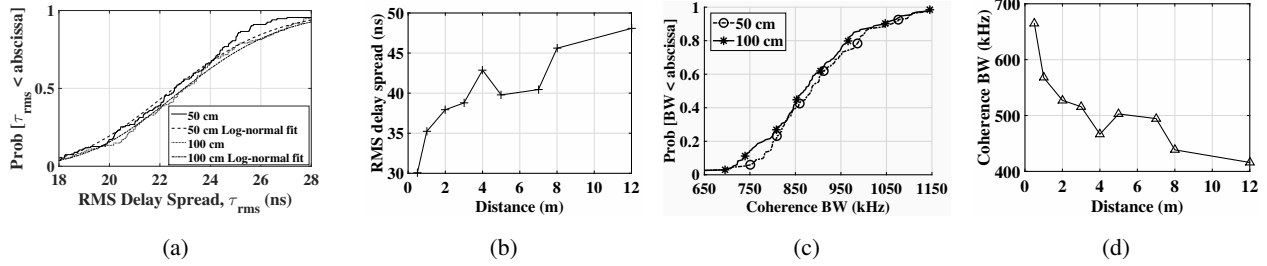| (a) | (b) | (c) | (d) |

Fig. 5: (a) Distribution of the RMS delay spread, τ_{rms}, for $50\,\text{cm}$ and $1\,\text{m}$ distance along with log-normal fit over all four depths in indoor testbed (silt loam) experiment, (b) The RMS delay spread, τ_{rms}, with distance in field (silty clay loam) experiment, (c) A distribution of coherence bandwidth for $50\,\text{cm}$ and $1\,\text{m}$ distance in indoor testbed (silt loam) experiment, (d) The coherence bandwidth with distance in field (silty clay loam) experiment.

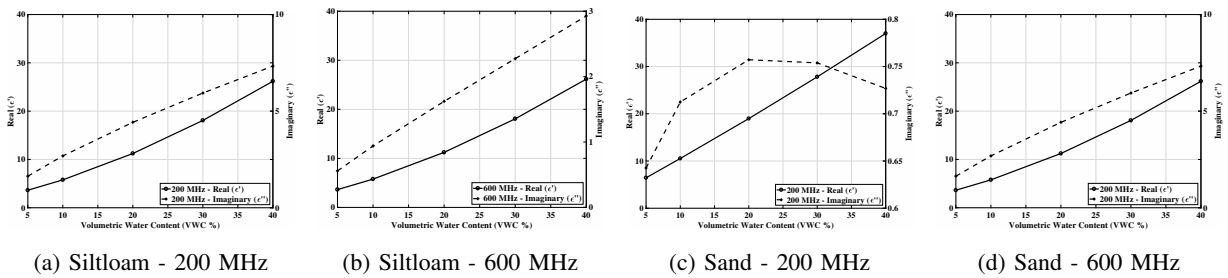| (a) Siltloam - 200 MHz | (b) Siltloam - 600 MHz | (c) Sand - 200 MHz | (d) Sand - 600 MHz |

Fig. 6: The dielectric constant of siltloam and sandy soil at $200\,\text{MHz}$ and $600\,\text{MHz}$ frequency.

range, VNA records 401 complex tones and stores them on external storage for post-processing. The discretized complex channel frequency response H_n is given by [67]:

$$\text{H}_n = \text{H}(f_{\text{start}} + n f_{\text{inc}}) \ , \tag{9}$$

where f_{start} and f_{inc} are the start and increment frequencies of the sweep, respectively. The n is number of evenly spaced data points across the frequency range. H_n is obtained by measuring the reference (R) and input (A) channels and taking the complex ratio, such that $\text{H}_n = \text{A}_n/\text{R}_n$. This process is repeated over the frequency range F_{sweep} at n discrete points, such that $f_{\text{inc}} = F_{\text{sweep}}/n$. To obtain channel impulse response, the complex frequency data is inverse Fourier transformed. The resulting N point complex channel impulse response has a delay bin spacing of $1/F_{\text{sweep}}$ and an unambiguous FFT range of N/F_{sweep}. The measured H_n are windowed using a minimum three term Blackman-Harris window [67] because of its excellent side lobe suppression and relatively wide main lobe width. Before time domain conversion, the windowing of H_n is required to avoid sinc^2 side lobes associated with rectangular nature of frequency sweep [67].

In Figs. 6, the dielectric constant in silt loam and sandy soil is shown at different frequency and

TABLE III: Mean (μ) and Standard Deviation (σ) in nanoseconds for the mean excess delay and the RMS delay spread in indoor testbed (silt loam) experiment.

| Depth | Mean Excess Delay τ | | | | RMS Delay Spread $\tau_{\mathbf{rms}}$ | | | |
| | 50 cm | | 1 m | | 50 cm | | 1 m | |
	μ	σ	μ	σ	μ	σ	μ	σ
10 cm	33.53	1.24	36.09	0.80	20.05	2.24	21.94	2.32
20 cm	34.66	1.07	37.12	1.00	24.93	1.64	25.10	1.77
30 cm	35.87	0.72	37.55	0.65	24.84	2.17	25.34	3.41
40 cm	36.43	0.74	40.18	0.94	23.91	2.84	25.62	1.87

water content values. It can be observed that ϵ'_s increases linearly when volumetric water content of the soil is increased. It can be observed that the imaginary part in Fig. 6(c) does not increase monotonically with volumetric water content. The dielectric constant of the soil depends on the many factors such as soil texture, volumetric water content, bulk density, frequency and particle density. At low frequency, $200\,\mathrm{MHz}$ in the sandy soil, the permittivity is not accurately predicted with Peplinski model, because the model does not work with sandy soil at lower frequencies with high sand content [21].

VI. ANALYSIS AND RESULTS

A. Characterization of UG Channel Impulse Response

The excess delay, mean access delay (7), the RMS delay spread (8) [66], [23], [9], and coherence bandwidth in relation to the RMS delay spread [16] are the parameters used to characterize the channel. For channel characterization, these parameters are used because system performance is not effected by the actual shape of PDP [66]. In the following, we discuss these metrics and the effects of soil moisture, soil types, distance, and depth on these metrics.

1) Statistics of Mean Excess Delay: Distribution of mean excess delay for $50\,\mathrm{cm}$ and $1\,\mathrm{m}$ distance over all four depths in indoor testbed (silt loam) experiment is given in Fig. 4(a). Higher mean excess delay can be observed with the increase in T-R separation, which corresponds to an increase of $2-3\,\mathrm{ns}\ (8\,\%)$. In Table III, statistics for mean (μ) and standard deviation (σ) for the mean excess delay for $50\,\mathrm{cm}$ and $1\,\mathrm{m}$ distances, and the 4 depths are shown. Higher mean excess delays are also observed as transmitter and receiver are buried deeper. In Fig. 4(b), excess delay is shown as a function of distance at $20\,\mathrm{cm}$ depth in field (silty clay loam) experiment. It can be observed that excess delay is increased from $40\,\mathrm{ns}$ up to $116\,\mathrm{ns}$ as UG communication distance increases from $50\,\mathrm{cm}$ to $12\,\mathrm{m}$.
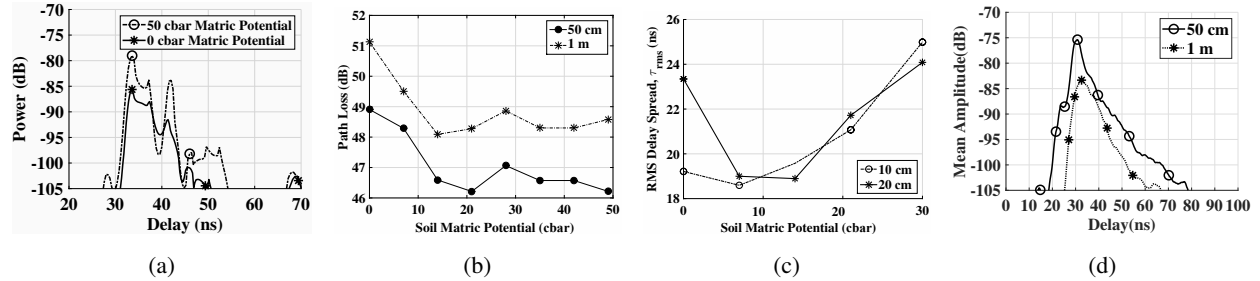
Fig. 7: Indoor testbed (silt loam) experiment: (a) Power delay profile, (b) Path loss with vs. soil moisture at 10 cm depth, (c) The RMS delay spread vs. soil moisture at 50 cm distance, (d) Mean amplitudes of all 50 cm and 1 m profiles across all depths.

2) Analysis of RMS Delay Spread: Distribution of the RMS delay spreads for T-R separations of $50\,\text{cm}$ and $1\,\text{m}$ in indoor testbed (silt loam) experiment, are shown in Fig. 5(a) with statistical fits. Our analysis shows that empirical distribution of τ_{rms} follows a log-normal distribution and the mean values of $23.94\,\text{ns}$ and $24.05\,\text{ns}$ and standard deviations of $3.7\,\text{ns}$ and $3.4\,\text{ns}$ for $50\,\text{cm}$ and $1\,\text{m}$ distance, respectively. In Table III, the statistics for mean (μ) and standard deviation (σ) of the RMS delay spread for $50\,\text{m}$ and $1\,\text{m}$ distances, and 4 depths are shown. It can be observed from Fig. 5(a) and Table III that the RMS delay spread (τ_{rms}) is dependent on T-R separation and burial depth with positive correlation. There is an increase of 2-3 ns ($20\,\%$) in the RMS delay spread as depth is increased from $10\,\text{cm}$ to $40\,\text{cm}$. A $4\,\text{ns}$ increase in the RMS delay spread can be observed from $10\,\text{cm}$ to $20\,\text{cm}$ depth at $50\,\text{cm}$ distance, which is caused by lateral wave, because at $20\,\text{cm}$ lateral wave reaches the receiver after direct wave. At $40\,\text{cm}$, the RMS delay spread decreases to $23\,\text{ns}$ because lateral wave attenuates more as the burial depth increases. In Fig. 5(b), the RMS delay spread is shown as a function of T-R distance at $20\,\text{cm}$ depth in field (silty clay loam) experiment. It can be observed that the RMS delay spread is increased to $48\,\text{ns}$ by increasing distance to $12\,\text{m}$.

The increase in the RMS delay spread with depth and distance is contributed by the strong multipaths associated with the lateral and reflected components, since their propagation time differences increase with distance. This increase in the RMS delay spread is an important result as it limits the system performance in terms of coherence bandwidth. It has been shown by analysis and simulations that maximum data rate that can be achieved without diversity or equalization is a few percent of the inverse of the RMS delay spread [16]. Using this relationship, a coherence bandwidth is established for the RMS delay spread. For our analysis, we have used $90\,\%$ signal correlation ($\frac{1}{50}\,\tau_{\text{rms}}$) as an approximation of coherence bandwidth, because underground channel experiences higher attenuation in soil as compared to terrestrial WSNs, where typically $50\,\%$ and $70\,\%$ signal correlation values are used to approximate coherence bandwidth.

In Fig. 5(c), the distribution of coherence bandwidth for $50\,\mathrm{cm}$ and $1\,\mathrm{m}$ distance over all depths in indoor testbed (silt loam) experiment is shown. It is observed that the range of coherence bandwidth for UG channel is between $650\,\mathrm{kHz}$ to $1.15\,\mathrm{MHz}$ for distances up to $1\,\mathrm{m}$. In Fig. 5(d), coherence bandwidth as a function of distance in field (silty clay loam) experiment is shown. It can be observed that the coherence bandwidth decreases to $418\,\mathrm{kHz}$ ($63\,\%$) as communication distance is increased to $12\,\mathrm{m}$. The restriction placed on the coherence bandwidth by the increase in the RMS delay spread with distance and depth should definitely be considered in system design but a fine design line should not be drawn because of the soil moisture variations, which are discussed next.

3) Soil Moisture Variations: In Fig. 7(a), the effect of soil moisture on amplitudes of a delay profiles is shown for $50\,\mathrm{cm}$ distance in indoor testbed (silt loam) experiment. Lower amplitudes can be observed for higher soil moisture (lower soil matric potential (cbar)) and this increase is consistent over all delay ranges. The amplitude decrease varies between $5-8\,\mathrm{dB}$ across the entire PDP.

Water in soil is classified into bound water and free water. Water contained in the first few particle layers of the soil is called bound water, which is strongly held by soil particles due to the effect of osmotic and matric forces [13]. Below these layers, effects of osmotic and matric forces is reduced, which results in unrestricted water movement. However, the presence of salinity can change the impact of osmotic potential (force) on soil-water movement dynamics substantially. EM waves experience dispersion when interfaced with bound water. Since permittivity of soil varies with time due to the variation in soil moisture, wavelength in soil changes which effects the attenuation that waves experience in soil.

In Fig. 7(b), the path loss with change in soil moisture (expressed as soil matric potential[4]) at $50\,\mathrm{cm}$ and $1\,\mathrm{m}$ distance and $10\,\mathrm{cm}$ depth in indoor testbed (silt loam) experiment is shown. The path loss decreases by $3-4\,\mathrm{dB}$ ($7\,\%$) as soil matric potential changes from 0 to $50\,\mathrm{cbar}$ (Centibars). In Fig. 7(c), change in the RMS delay spread with change in soil moisture at $50\,\mathrm{cm}$ distance, $10\,\mathrm{cm}$ and $20\,\mathrm{cm}$ depth in indoor testbed (silt loam) experiment is shown. From near-saturation to $8\,\mathrm{cbar}$, the RMS delay spread has decreased first and then increases as soil moisture decreases. This is attributed to water repellency of soil particles where infiltration is slowed momentarily at near-saturation levels. For $10\,\mathrm{cm}$ depth, the RMS delay spread has increased

---

[4]Greater matric potential values indicate lower soil moisture and zero matric potential represents near saturation condition.
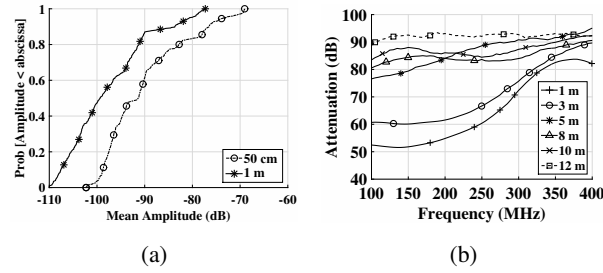
Fig. 8: Indoor testbed (silt loam) experiment: (a) Distribution function of mean amplitudes at $40\,\mathrm{cm}$ depth. Field (silty clay loam) experiment: (b) Attenuation with frequency.

from $19\,\mathrm{ns}$ to $25\,\mathrm{ns}$ ($31\,\%$) as soil moisture decreases. Similar increase in the RMS delay spread with decrease in soil moisture can be observed for $20\,\mathrm{cm}$ depth. The low water absorption of EM waves with decrease in soil moisture contributes to increase in τ_{rms} as multipath components exhibit less attenuation.

The variations in amplitudes and path loss with the change in soil moisture lead to changes in coherence bandwidth, optimal system capacity and communication coverage range. Specifically, increase in the RMS delay spread with soil moisture decreases coherence bandwidth of the channel, and attenuation is also increased when soil moisture increases. Therefore, the underground communication devices should have the ability to adjust their operation frequency, modulation scheme, and transmit power to compensate these changes caused by soil moisture variation. The cognitive radio [4] solutions can be used to adopt parameters based on changing channel conditions.

4) Soil Type: Soils are divided into textural classes based on their particle size. To analyze the effects of soil texture, we have measured the channel statistics for silty clay loam, silt loam, and sandy soils. In Table IV, statistics of mean (μ) and standard deviation (σ) for the mean excess delay, the RMS delay spread and path loss for $50\,\mathrm{cm}$ and $1\,\mathrm{m}$ distances, and 4 depths

TABLE IV: Mean (μ) and Standard Deviation (σ) for the Mean Excess Delay, the RMS delay spread and Path Loss for $50\,\mathrm{cm}$ and $1\,\mathrm{m}$ distances, and $20\,\mathrm{cm}$ depth for three soils. Values are in nanoseconds.

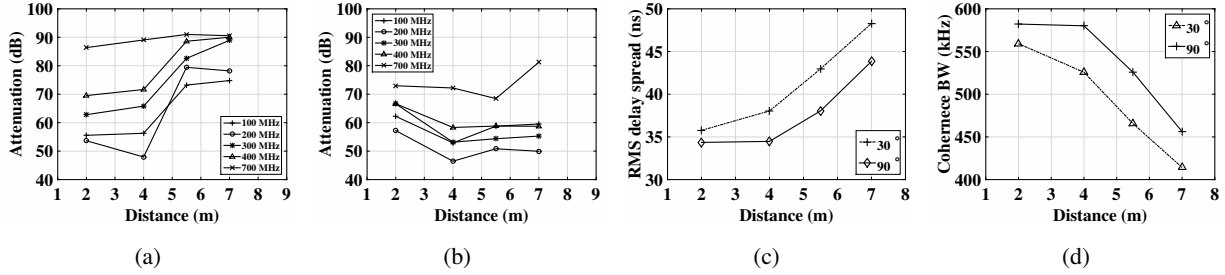| Soil Type	Mean Excess Delay				RMS Delay Spread				Path Loss	
	Distance				Distance				Distance	
	50 cm		1 m		50 cm		1 m		50 cm	1 m
	μ	σ	μ	σ	μ	σ	μ	σ		
Silty Clay Loam	34.77	2.44	38.05	0.74	25.67	3.49	26.89	2.98	49 dB	52 dB
Silt Loam	34.66	1.07	37.12	1.00	24.93	1.64	25.10	1.77	48 dB	51 dB
Sandy Soil	34.13	1.90	37.87	0.80	27.89	2.76	29.54	1.66	40 dB	44 dB

Fig. 9: The attenuation with distance at different receiver angles (UG2AG) : (a) 0°, (b) 90°, (c) The RMS delay spread with distance, (d) The coherence bandwidth with distance.

are shown.

the RMS delay spread τ_{rms} in sandy soil is $2\,\mathrm{ns}$ higher than silty clay loam, which is $1\,\mathrm{ns}$ higher than the silt loam on the average. Similarly, path loss is $4-5\,\mathrm{dB}$ lower in sandy soil as compared to silt loam and silty clay loam. This is due to the lower attenuation in sandy soil. Attenuation of EM waves in soil varies with soil type [10]. Sandy soil holds less bound water, which is the major component in soil that absorbs EM waves. Water holding capacity of fine-textured (silt-loam, silty clay loam) and medium-textured soils (fine sandy loam) is much higher, because of the small pore size (but, greater number of pores), as compared to coarse-textured (sandy, sandy loam, loamy sand) because of larger pore size (but less in number of pores) [13]. Hence the soils containing the highest clay contents suffer more attenuation.

In sandy soil, there is a trade-off between attenuation and the RMS delay spread. The RMS delay spread τ_{rms} is large due to least attenuated multipath components arriving at the receiver with large delays. On the other hand, overall attenuation is low as compared to silt loam and silty clay loam. Therefore, the higher SNR can be achieved with moderate coherence bandwidth. Effects of soil texture must be taken into account during design and deployment of WUSNs and optimal system parameters such as communication range and data rates should be selected based on the physical characteristics of the soil.

TABLE V: Speed of the wave in all three soils, calculated by refractive indices n based on particle size distribution of soils given in Table II.

Soil Type	Speed in the Soil m/s	% of C	Refractive Index n
Silt Loam	$5.66\mathrm{x}10^7$	18.89	5.28
Sandy Soil	$5.01\mathrm{x}10^7$	16.71	5.98
Silty Clay Loam	$5.67\mathrm{x}10^7$	18.91	5.29

5) Distance and Depth: The communication in UG channel is effected by depth and T-R separation. However, these impacts are much more severe then over the air communication. In Fig. 7(d), effects of T-R distance are shown in indoor testbed (silt loam) experiment. By increasing the distance from $50\,cm$ to $1\,m$, the first component in the $1\,m$ PDP is delayed by $10\,ns$. An $8\,dB$ difference in peak amplitude is observed between profiles at $50\,cm$ and $1\,m$. Distribution of mean amplitudes of $50\,cm$ and $1\,m$ profiles at $40\,cm$ depth in indoor testbed (silt loam) experiment is shown in Fig. 8(a). A $9-10\,dB$ decrease in mean amplitude can be observed when T-R separation is increased from $50\,cm$ to $1\,m$. Peak amplitude of delay profile is decreased by $5\,dB$ from $10\,cm$ depth to $40\,cm$ depth at $50\,cm$ distance, whereas this decrease in peak amplitude is $20\,dB$ for $1\,m$ distance when depth is changed from $10\,cm$ to $40\,cm$. Since increase in burial depth increases the path of EM waves in soil, higher attenuation is observed.

EM waves in soil are reflected and attenuated by soil-air interface and suffers diffusion attenuation. Additional attenuation is caused by absorption of waves in soil. Higher attenuation is the limiting factor for communication system design. The attenuation is increased with distance and depth because of reflection effects of lateral wave. At soil-air interface phase of lateral wave is randomly changed, which adds constructive-destructive interference at the receiver.

6) Operation Frequency: In Fig. 8(b), the attenuation with frequency at different distances of up to $12\,m$ are presented. Transmitter and receiver depths are set to $20\,cm$. At $2\,m$ distance, attenuation increases by $24\,dB$ when frequency increases from $200\,MHz$ to $400\,MHz$. Similarly, for $200\,MHz$, attenuation is increased from $51\,dB$ to $92\,dB$ ($80\,\%$) when distance increases from $50\,cm$ to $12\,m$.

Higher frequencies suffer more attenuation because when EM waves propagate in the soil their wavelength shortens due to higher permittivity of soil than the air. Hence, due to less effects of permittivity of soil on lower frequency spectrum, it is more suitable for UG2UG communication as larger communication distances can be achieved. In order to have minimum attenuation, an operation frequency should be selected, for each distance and depth, such that attenuation is minimized. This is important from WUSN topology design perspective because deployment needs to customized to the soil type and frequency range of sensors being used for deployment. These results form the basis of the statistical model of UG channel developed in Section. VII.

VII. STATISTICAL MODEL, EVALUATION AND EXPERIMENTAL VERIFICATION

To engineer an underground communication system, a statistical model of propagation in the wireless underground channel can help in optimizing system performance, designing tailored modulated/coding schemes, and in end-to-end capacity analysis. For example, received data signals can be detected coherently in the absence of ISI. In this section a detailed characterization of the underground channel is done based on the measurements of Section VI. The multipath profiles taken in different soils under different soil moisture levels are analyzed to perform statistical analysis of experimental data.

A. The Statistical Model

To model the wireless underground channel, our approach follows the standard OTA modeling approaches described in [15], [23], [66], and [76], with modifications due to unique nature of wireless propagation in the underground channel. Based on the measurement analysis, the following assumptions are made:

1) The correlation among multipath components at different delays in the lateral, reflected, and direct component is very small and negligible for all practical purposes. However multipaths within each component are affected by the strongest path and hence are correlated. Therefore, the tap-delay-lines are assumed uniformly spaced within each component.

2) At the receiver, phases are completely random with uniform distribution over $[0, 2\pi)$.

To keep model tractable, arrival rate of delays within each component is kept constant, and amplitudes of these multipaths in each component are statistically independent. This helps in modeling the physical characteristics of the UG channel and provide ease of analysis without losing insight into delay statistics. The order of the arrival of the lateral, direct, and reflected component depends upon the burial depth, and distance between transmitter-receiver (T-R), because the path traversal through soil and air exhibits different wave propagation speeds depending on the soil characteristics, and soil moisture level. Only for the T-R distances less than $50\,\mathrm{cm}$, the direct component arrives first, and as the distance increases, the lateral component reaches at the receiver first due to higher propagation speed in the air medium. Due to significant differences in speed of the three components in soil and air mediums, no component overlap is observed, and the power of multipaths (gain) within each component decays before the arrival of the next component. Moreover, in our measurements, there were not any significant detectable components observed beyond the $100\,\mathrm{ns}$ time delay.
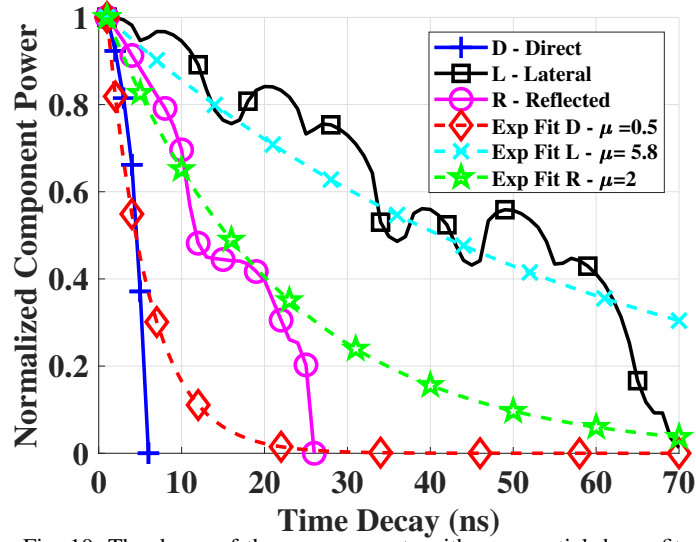
Fig. 10: The decay of three components with exponential decay fit.

Next, statistics of amplitudes α_{li}, α_{dj}, and α_{rk} at delays τ_{li}, τ_{di}, and τ_{ri} for lateral, direct, and reflected waves, respectively, are derived. In Fig. 10, the mean amplitudes of a profile have been shown at $50\,\mathrm{cm}$ distance with exponential decay fit. The analysis of the measurement data shows that gains of multipaths within each component follow the exponential decay. Therefore, the path amplitudes of the three components are modeled as decaying exponentials within each component. The multipath amplitudes calculated from the arrival time τ_L, decay rate γ_L, and amplitude α_L of the lateral component. It is given as [66]

$$\alpha_{li} = \alpha_{l0}e^{-(i-\tau_L)/\gamma_L} \ \forall \ i > \tau_l \text{ and } i < \tau_l + \mathrm{L}. \tag{10}$$

The α_{dj} for the direct component is obtained from the arrival time τ_D, decay rate γ_D, and amplitude α_D of the direct component. It is expressed as:

$$\alpha_{dj} = \alpha_{d0}e^{-(j-\tau_D)/\gamma_D} \ \forall \ j > \tau_d \text{ and } j < \tau_d + \mathrm{D}. \tag{11}$$

Similarly, for the reflected component, α_{rk} is given as:

$$\alpha_{rk} = \alpha_{r0}e^{-(k-\tau_R)/\gamma_R} \ \forall \ k > \tau_r \text{ and } k < \tau_r + \mathrm{R}. \tag{12}$$

Gain of first multipath is denoted as α_{d0}, α_{l0}, and α_{r0}. These multipaths within each components

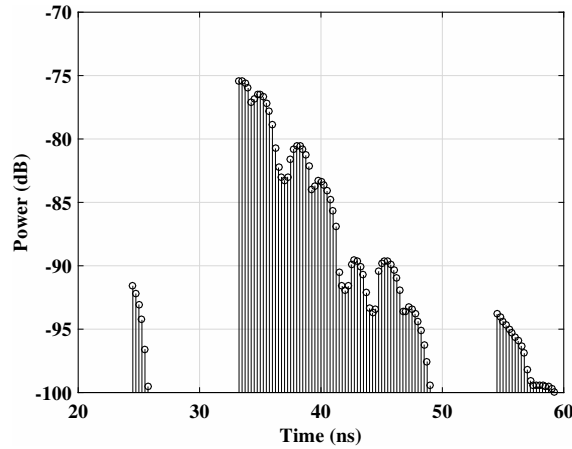Fig. 11: A realization of wireless underground channel impulse response

are calculated as follows [11]:

$$\alpha_{\text{d}0} = P_t + 20 \log_{10} \lambda_s - 20 \log_{10} r_1 - 8.69 \alpha_s r_1$$

$$-22 + 10 \log_{10} D_{rl} \ ,$$

$$\alpha_{\text{r}0} = P_t + 20 \log_{10} \lambda_s - 20 \log_{10} r_2 - 8.69 \alpha_s r_2$$

$$+20 \log_{10} \Gamma - 22 + 10 \log_{10} D_{rl} \ , \tag{13}$$

$$\alpha_{\text{l}0} = P_t + 20 \log_{10} \lambda_s - 40 \log_{10} d - 8.69 \alpha_s (h_t + h_r)$$

$$+20 \log_{10} T - 22 + 10 \log_{10} D_{rl} \ ,$$

where P_t is the transmitted power, Γ and T are reflection and transmission coefficients [11], respectively, r_2 is the length of the reflection path, $r_1 = \sqrt{(h_t - h_r)^2 + d^2}$, $r_2 = \sqrt{(h_t + h_r)^2 + d^2}$, where h_t and h_r are transmitter and receiver burial depth, and λ_s is the wavelength in soil [30].

In the statistical model, exponential decay is justified because the time delay depends on the travel paths, and the path gains are affected by the soil. Therefore, the gains of the successive multipaths depends on the delay of those multipaths. It is also important to note that, in addition to the soil moisture, the multipath gains $\alpha_{\text{l}i}$, $\alpha_{\text{d}j}$, and $\alpha_{\text{r}k}$ are also impacted by soil type. For example, in sandy soils, path gains are much higher due to lower attenuation as compared to the silt loam and silty clay loam soils due to the less water absorption of EM waves in sandy. This is attributed to the low water holding capacity of sandy soils. However, soil type impact on multipaths gains $\alpha_{\text{l}i}$, $\alpha_{\text{d}j}$, and $\alpha_{\text{r}k}$ does not require separate modeling in (10) - (12). Therefore,

TABLE VI: The impulse response model parameters.

Parameter	Description	Model	Values
S	Speed of wave in soil [62]	C/η	C= 3×10^8
η	Refraction Index [62]	$\eta = \sqrt{\sqrt{\epsilon'^2 + \epsilon''^2} + \epsilon'/2}$	ϵ', ϵ''
ϵ'	Real part of relative permittivity of the soil [21]	$\epsilon'_s = \begin{cases} 1.15\left[1 + \rho_b/\rho_s\left(\epsilon_s^\delta - 1\right) + (m_v)^{\nu'}(\epsilon'_{fw})^\delta - m_v\right]^{1/\delta} - 0.68 \quad 0.3\,\text{GHz} \leq f \leq 1.4\,\text{GHz} , \\ \left[1 + \rho_b/\rho_s\left(\epsilon_s^\delta - 1\right) + (m_v)^{\nu'}(\epsilon'_{fw})^\delta - m_v\right]^{1/\delta} \\ \qquad\qquad 1.4\,\text{GHz} \leq f \leq 18\,\text{GHz} , \end{cases}$	S = Sand in %, C= Clay in %, $\delta = 0.65$, $\nu' = 1.2748 - 0.519S - 0.152C$, $\nu'' = 1.33797 - 0.603S - 0.166C$ ϵ'_{fw}, ϵ''_{fw}
ϵ''	Imaginary part of relative permittivity of the soil [21]	$\epsilon''_s = \left[(m_v)^{\nu''}(\epsilon''_{fw})^\delta,\right]^{1/\delta}$	
ϵ'_{fw}	Real part of relative permittivity of the free water [21]	$\epsilon'_{fw} = e_{w\infty} + \frac{\epsilon_{w0} - \epsilon_{w\infty}}{1 + (2\pi f \tau_w)^2}$	$\epsilon_{w\infty} = 4.9$ is the limit of ϵ'_{fw} when $f \to \infty$, ϵ_{w0} is the static dielectric constant for water, τ_w is the relaxation time for water, and ϵ_0 is the permittivity of free space. At room temperature, $2\pi\tau_w = 0.58 \times 10^{-10}s$ and $\epsilon_{w0} = 80.1$, effective conductivity, δ_{off}
ϵ''_{fw}	Imaginary part of relative permittivity of the free water [21]	$\epsilon''_{fw} = \frac{2\pi, f\tau_w(\epsilon_{w0} - \epsilon_{w\infty})}{1 + (2\pi, f\tau_w)^2} + \frac{\delta_{eff}}{,2\pi\epsilon_0 f}\frac{(\rho_s - \rho_b)}{\rho_s m_v}$	
δ_{eff}	Effective conductivity of soil [21]	$\delta_{eff} = \begin{cases} 0.0467 + 0.2204\rho_b - 0.4111S + 0.6614C \\ \qquad\qquad 0.3\,\text{GHz} \leq f \leq 1.4\,\text{GHz} . \\ -1.645 + 1.939\rho_b - 2.25622S + 1.594C \\ \qquad\qquad 1.4\,\text{GHz} \leq f \leq 18\,\text{GHz} \end{cases}$	ρ_b is bulk density
τ_d	Arrival time of direct component	$\tau_d = (\delta_s/S)$	S is speed of wave in soil
τ_r	Arrival time of reflected component	$\tau_r = 2 \times (\delta_s/S)$	S is speed of wave in soil
τ_l	Arrival time of reflected component	$\tau_l = 2 \times (\delta_s/S) + (\delta_a/c)$	S is speed of wave in soil C is speed of wave in air
α_{d0}, α_{r0}, α_{l0},	Gains of the three main components	$\alpha_{d0} = P_t + 20\log_{10}\lambda_s - 20\log_{10} r_1 - 8.69\alpha_s r_1$ $-22 + 10\log_{10} D_{rl}$ $\alpha_{r0} = P_t + 20\log_{10}\lambda_s - 20\log_{10} r_2 - 8.69\alpha_s r_2$ $+20\log_{10}\Gamma - 22 + 10\log_{10} D_{rl}$ $\alpha_{l0} = P_t + 20\log_{10}\lambda_s - 40\log_{10} d - 8.69\alpha_s(h_t + h_r)$ $+20\log_{10} T - 22 + 10\log_{10} D_{rl}$, See also analysis from Table VI.	μ and σ
α_{di}, α_{rj}, α_{lk}	Path amplitudes of the three components	$\alpha_{li} = \alpha_{l0}e^{-(i-\tau_L)/\gamma_L} \,\forall,\ i > \tau_l$ and $i < \tau_l + $L $\alpha_{dj} = \alpha_{d0}e^{-(j-\tau_D)/\gamma_D} \,\forall,\ j > \tau_d$ and $j < \tau_d + $D $\alpha_{rk} = \alpha_{r0}e^{-(k-\tau_R)/\gamma_R} \,\forall,\ k > \tau_r$ and $k < \tau_d + $R	

it is captured in the main lateral, direct, and reflected components α_{l0}, α_{d0}, and α_{r0} and is propagated to α_{li}, α_{dj}, and α_{rk} in (10) - (12) due to their dependence on α_{l0}, α_{d0}, and α_{r0}.

Next, number of significant paths are determined. Number of multipaths L, D, and R in each of the components are determined by setting a gain threshold (paths within $30\,\text{dB}$ from peak).
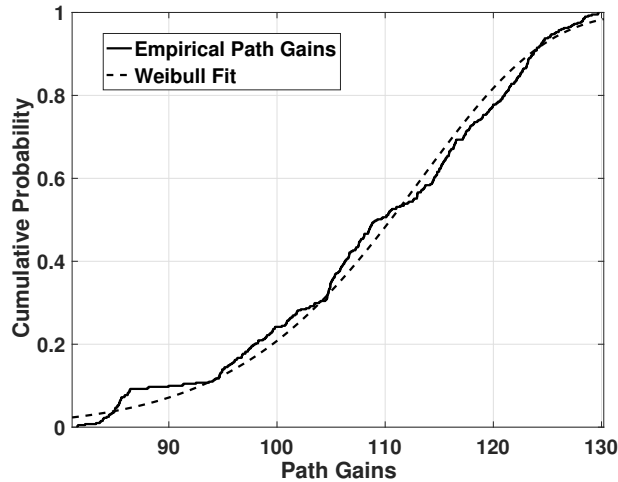
Fig. 12: Amplitude gains with Weibull distribution fit.

Multipath generation in a particular component is stopped once the path amplitude in that bin falls below the threshold value. This results in larger number for the sandy soils, and lower number of multipaths for silt loam, and silty clay loam soils which is also in good agreement with empirical observations. Moreover, this number being an indicator of the channel spread, also depends on the soil moisture. The higher soil moisture leads to lower spread, and on the other hand lower soil moisture decrease attenuation, which leads to emergence of higher number of multipaths falling above the threshold value and higher number of multipaths. A realization of underground channel impulse response model is shown in Fig. 11. The model parameters are shown in Table VI.

Up to this point, $\alpha_{l,i}$, $\alpha_{d,i}$, and $\alpha_{r,i}$ are calculated based on the delays within lateral, reflected,

---

Algorithm 1 UG Channel Impulse Response Simulation

1: *Initialization* :

2: Input soil parameters

3: Obtain the soil moisture level

4: **BEGIN**

5: Generate the decay exponents for the lateral, direct, and reflected components

6: Determine the arrival time

7: Calculate the first multipath gain of each of the three components

8: Generate the multipaths and impulse response

9: **END**

TABLE VII: The validation of impulse response model parameters.

Impulse Response Parameter	Measured	Modeled
RMS Delay Spread (τ_{rms})	$45.52\,\mathrm{ns}$	$38.84\,\mathrm{ns}$
Coherence Bandwidth	$439\,\mathrm{kHz}$	$514\,\mathrm{kHz}$

and direct components which depends on the exponential decay of multipath with respect to the main path gain in each component. This is a good realization of physical measurements. However, if we normalize the path gains with each components by average of these gains such that $\alpha_{\mathrm{l}i}/\bar{\alpha}_{\mathrm{l}i}$, $\alpha_{\mathrm{d}j}/\bar{\alpha}_{dj}$, and $\alpha_{\mathrm{r}k}/\bar{\alpha}_{rk}$, then, these amplitudes become independent of the delays to which these are associated [66]. Accordingly, a commutative distribution of path gains normalized through this process is shown in Fig. 12, which follows the Weibull probability distribution.

B. Model Evaluation

The model parameters required to evaluate the statistical model are summarized in the Table VI. In the numerical evaluation, first, we need to find the the $\alpha_{\mathrm{l}i}$, $\alpha_{\mathrm{d}j}$, and $\alpha_{\mathrm{r}k}$ and their associated delays $\tau_{\mathrm{l}i}$, $\tau_{\mathrm{d}i}$, and $\tau_{\mathrm{r}i}$. After generating the delays and amplitudes of these three components, other impulse response parameters are found and compared with the measurement data. An algorithm to generate UG channel impulse response is shown in Algorithm 1.

The simulation algorithm takes soils parameters such as soil type, and soil moisture as input and calculates the arrival times of the direct, reflected, and lateral components, τ_{d}, τ_{r} and τ_{l}. Based on the soil type, peak power gains $\tau_{\mathrm{d}0}$, $\tau_{\mathrm{r}0}$, $\tau_{\mathrm{l}0}$, are determined from the Table VI. The model parameters for peak amplitude, delays, and number of multipaths statistics for direct, lateral and reflected components for three soil types are given in [62, Table VI].

The different statistical parameters computed from the measurement data, and the channel model numerical evaluations are compared in Table VII. UG channel is evaluated numerically using the the statistical model. The RMS delay spread and the coherence bandwidth parameters are derived and compared with the parameters obtained through experimental data. Model prediction error for the RMS delay spread is 14.67%, and for the the coherence bandwidth, it is 14.08%. It can be observed that the difference in predicted and measured values, which is due to model uncertainty and observational error, is less than 15%. Overall, the developed statistical model shows a good agreement with the empirical data, and statistics of the coherence bandwidth and the RMS delay spread prove the validity of the statistical model.
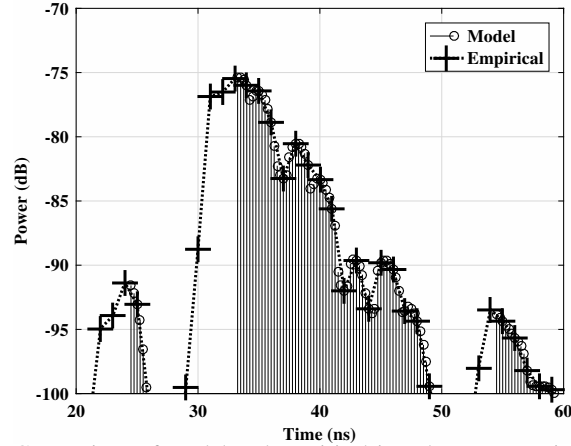
Fig. 13: Comparison of model and empirical impulse response in silt loam.

C. Empirical Validation

A good statistical model should be able to simulate the empirical measurements with higher accuracy. Moreover, simulated response must have the same characteristics as of the measurements results. In this section, arrival of multipath components is validated with experiments conducted in the indoor testbed. Moreover, the shape of the PDP is presented and physical interpretations are discussed.

The speed of the wave in all three soils is found by calculating the refractive indices n based on particle size distribution and classification of soils given in Table I. The results of these calculations are shown in Table V. In Fig. 13, a measured PDP for a silt loam at $40\,cm$ depth is compared with a schematic representation of the 3-wave model for T-R separation of $50\,cm$. Analysis of arrival time of three components reveals that for $50\,cm$ distance and all burial depths, lateral waves arrive later than the direct wave except for the $10\,cm$ depth where lateral wave reaches the receiver first. It can be observed that measurement data shows a strong agreement with the model.

From Fig. 13, it can also be observed that lateral component is the strongest component compared to the direct and reflected components. This is because direct and reflected components are spherical waves, propagating radially outward from the antenna, whereas, the lateral component is, initially, a plane wave that travels upward from the source to the boundary, then horizontally as a cylindrical wave, and subsequently travels backward as a plane wave from boundary to the point of observation. The proposed model is applicable to different environments for wireless underground communications. Accordingly, tailored sensing, control, and communication strategies can be developed.

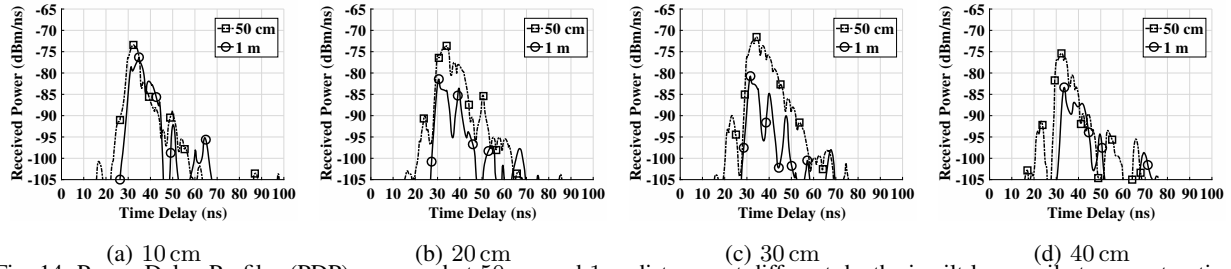(a) 10 cm   (b) 20 cm   (c) 30 cm   (d) 40 cm

Fig. 14: Power Delay Profiles (PDP) measured at 50 cm and 1 m distance, at different depths in silt loam soil at near-saturation: (a) 10 cm, (b) 20 cm, (c) 30 cm, (d) 40 cm.
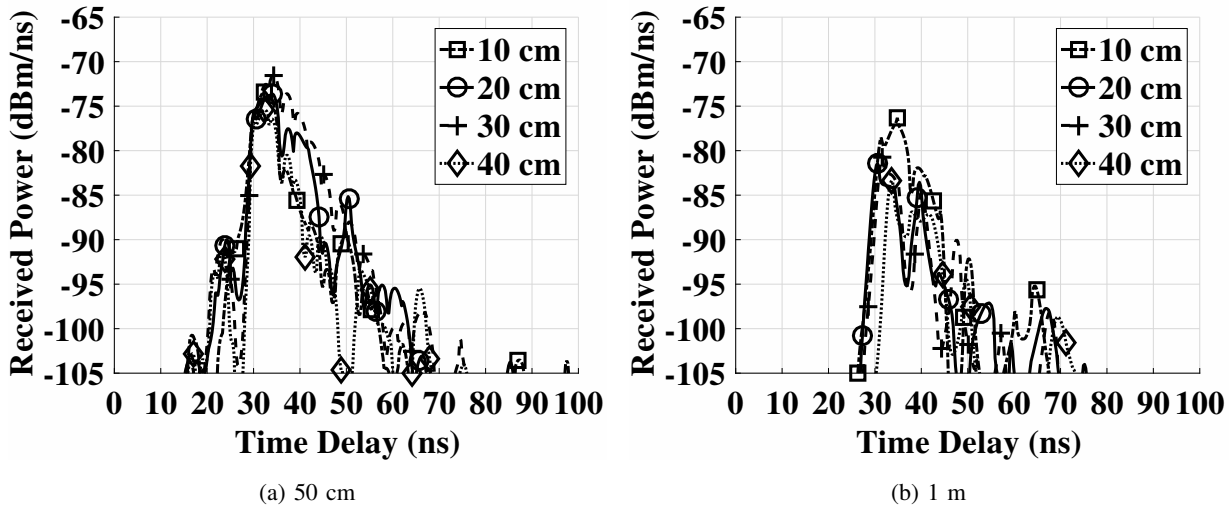

(a) 50 cm   (b) 1 m

Fig. 15: The power delay profile in silt loam soil at different depths at: (a)) 50 cm T-R distance, (b)) 1 m T-R distance.

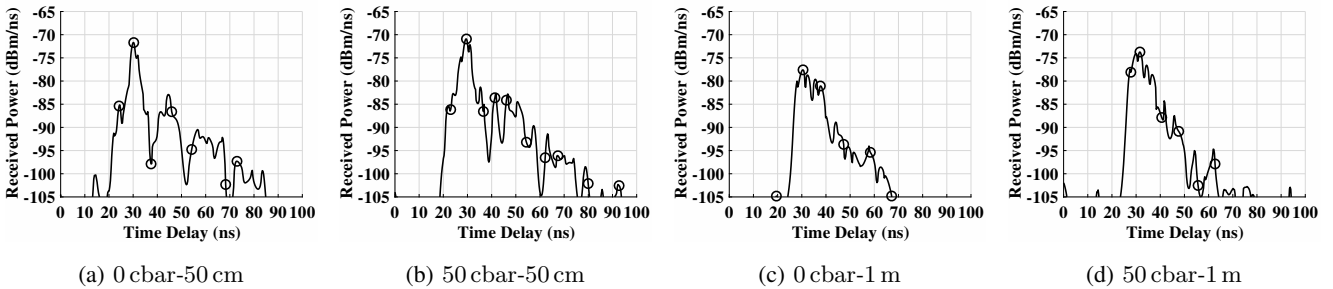(a) 0 cbar-50 cm   (b) 50 cbar-50 cm   (c) 0 cbar-1 m   (d) 50 cbar-1 m

Fig. 16: Power Delay Profiles (PDP) measured at 50 cm and 1 m distance, at 20 cm depths for different soil moisture levels: (a)) 0 cbar-50 cm, (b)) 50 cbar-50 cm, (c)) 0 cbar-1 m, (d)) 50 cbar-1 m.

VIII. THE POWER DELAY PROFILE MEASUREMENTS

In this section, we present the underground channel impulse response measurements. In Fig. 14, PDPs of 50 cm and 1 m distances are compared for all depths. The first multipath component shown in the PDPs is the direct wave component, which is present at $18-28$ ns delay at 50 cm profile and it is not formed at 1 m profile. This is because direct wave suffers less attenuation at 50 cm and more attenuated at 1 m distance. It is observed that the lateral wave component is the strongest in all power delay profiles and is formed at $30-40$ ns delay. The delays of the lateral
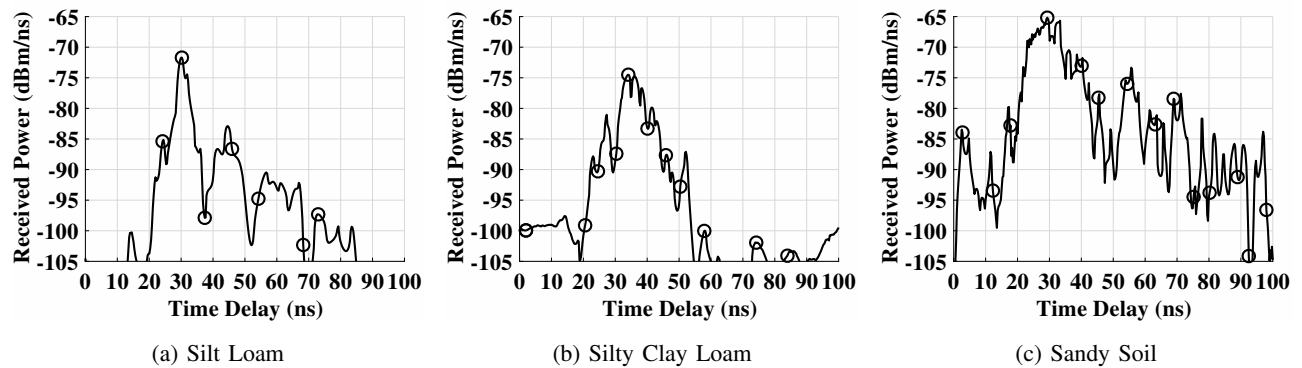
Fig. 17: The Power Delay Profiles (PDP) measured in different soils: (a) Silt Loam, (b) Silty Clay Loam, (c) Sandy Soil.

wave is both $50\,\mathrm{cm}$ and $1\,\mathrm{m}$ distances are similar because the wave propagates much faster in air. In general, the lateral wave component is $10\,\mathrm{dB}$ to $15\,\mathrm{dB}$ higher in power than the direct wave component.

In Fig. 15, PDPs of the communication channels at four depths are compared. In Fig. 15(a), the distance between the transmitter and the receiver is $50\,\mathrm{cm}$, while in Fig. 15(b) the distance is $1\,\mathrm{m}$. As shown in figures, at the same distance, with the increase of the depth, the received power of lateral wave decreases. This is more significant in the $1\,\mathrm{m}$ case, where the peak power of the lateral wave in the $10\,\mathrm{cm}$ depth is $-75\,\mathrm{dB}$ while it is $-83\,\mathrm{dB}$ when the depth increases to $40\,\mathrm{cm}$. Also shown in Fig. 15(b), with the increase of the depth, the component delay also increases. At $10\,\mathrm{cm}$ depth, the lateral wave arrives at $29\,\mathrm{ns}$ while at $40\,\mathrm{cm}$ it arrives at $32\,\mathrm{ns}$. Distance related delay of $10-15\,\mathrm{ns}$ can be also observed in all profiles at $1\,\mathrm{m}$ distance.

In Fig. 16, the PDP measured at $50\,\mathrm{cm}$ and $1\,\mathrm{m}$ distance, at $20\,\mathrm{cm}$ depths for different soil moisture levels are shown. It can be observed that at $50\,\mathrm{cm}$ distance, with decrease in soil moisture, the received power is increased and also the components at longer delay exhibit more strength. Similar observations are made at 1m distance. It is also important to note that direct component vanishes as distance increase, which is caused by the higher attenuation in the soil. In Fig. 17, the measured PDPs in different soils are shown. It can be observed that due to the low water holding capacity of the sandy soil, it has higher received power across all three components as compared to the silt loam and silty clay loam soil.

IX. CONCLUSION

In this paper, analysis of impulse response of wireless underground channel is presented. A 3-wave based impulse response model of underground channel is developed and validated with

measured data. Distribution of mean excess delay and the RMS delay spread is determined and it is shown that the RMS delay spread is log-normally distributed. Effect of T-R separation on mean amplitudes of power delay profile is showed. We have presented the impact of soil moisture and soil types on the RMS delay spread and power gains of delay profiles. It is presented that the RMS delay spread increases with increase in soil moisture. It is also showed that coarse-textured soils have larger the RMS delay spreads and lower attenuation as compared to fine and medium-textured soils. Coherence bandwidth of UG channel in relation to the RMS delay spread is modeled and showed to be less than $1\,\mathrm{MHz}$. Coherence bandwidth findings reveled the use of OFDM for underground channel communication to have ISI free communication and for significant performance improvements. These findings serve as important characterization parameters of UG channel and give guidelines for design of an underground communication system.

X. ACKNOWLEDGMENTS

REFERENCES

[1] P. Abouzar, D. G. Michelson, and M. Hamdi, "Rssi-based distributed self-localization for wireless sensor networks used in precision agriculture," *IEEE Transactions on Wireless Communications*, vol. 15, no. 10, pp. 6638–6650, Oct 2016.

[2] T. E. Abrudan, O. Kypris, N. Trigoni, and A. Markham, "Impact of rocks and minerals on underground magneto-inductive communication and localization," *IEEE Access*, vol. 4, pp. 3999–4010, 2016.

[3] M. A. Akkaş, "Channel modeling of wireless sensor networks in oil," *Wireless Personal Communications*, pp. 1–19, 2017. [Online]. Available: http://dx.doi.org/10.1007/s11277-017-4083-9

[4] I. F. Akyildiz and et.al., "Next generation/dynamic spectrum access/cognitive radio wireless networks: A survey," *Computer Networks Journal, (Elsevier)*, vol. 50, pp. 2127–2159, September 2006.

[5] I. F. Akyildiz, Z. Sun, and M. C. Vuran, "Signal propagation techniques for wireless underground communication networks," *Physical Communication Journal (Elsevier)*, vol. 2, no. 3, pp. 167–183, Sept. 2009.

[6] A. Bicen, A. Sahin, and O. Akan, "Spectrum-aware underwater networks: Cognitive acoustic communications," *Vehicular Technology Magazine, IEEE*, vol. 7, no. 2, pp. 34–40, June 2012.

[7] H. R. Bogena and et.al., "Hybrid wireless underground sensor networks: Quantification of signal attenuation in soil," *Vadose Zone Journal*, vol. 8, no. 3, pp. 755–761, August 2009.

[8] H. R. Bogena and et.al., "Potential of wireless sensor networks for measuring soil water content variability," *Vadose Zone Journal*, vol. 9, no. 4, pp. 1002–1013, November 2010.

[9] D. Cassioli, M. Win, and A. Molisch, "The ultra-wide bandwidth indoor channel: from statistical model to simulations," *IEEE JSAC*, vol. 20, no. 6, pp. 1247–1257, Aug 2002.

[10] M. Dobson and et.al., "Microwave dielectric behavior of wet soil—Part II: Dielectric mixing models," *IEEE Trans. Geoscience and Remote Sensing*, vol. GE-23, no. 1, pp. 35 –46, January 1985.

[11] X. Dong and M. C. Vuran, "A channel model for wireless underground sensor networks using lateral waves," in *Proc. of IEEE Globecom '11*, Houston, TX, December 2011.

[12] X. Dong, M. C. Vuran, and S. Irmak, "Autonomous precision agricultrue through integration of wireless underground sensor networks with center pivot irrigation systems," *Ad Hoc Networks (Elsevier)*, 2012.

[13] H. D. Foth, *Fundamentals of Soil Science*, 8th ed. John Wiley and Sons, 1990.

[14] H. Guo and Z. Sun, "Channel and energy modeling for self-contained wireless sensor networks in oil reservoirs," *Wireless Communications, IEEE Transactions on*, vol. 13, no. 4, pp. 2258–2269, April 2014.

[15] H. Hashemi, "Impulse response modeling of indoor radio propagation channels," *IEEE Journal on Selected Areas in Communications*, vol. 11, no. 7, pp. 967–978, Sep 1993.

[16] S. Howard and K. Pahlavan, "Measurement and analysis of the indoor radio channel in the frequency domain," *Instrumentation and Measurement, IEEE Transactions on*, vol. 39, no. 5, pp. 751–755, Oct 1990.

[17] M. N. Islam, B. J. Kim, P. Henry, and E. Rozner, "A wireless channel sounding system for rapid propagation measurements," in *Proc. IEEE ICC' 2013*, Jun. 2013, pp. 5720–5725.

[18] R. W. P. King, M. Owens, and T. T. Wu, *Lateral Electromagnetic Waves*. Springer-Verlag, May 1992.

[19] A. Konda, A. Rau, M. A. Stoller, J. M. Taylor, A. Salam, G. A. Pribil, C. Argyropoulos, and S. A. Morin, "Soft microreactors for the deposition of conductive metallic traces on planar, embossed, and curved surfaces," *Advanced Functional Materials*, vol. 28, no. 40, p. 1803020. [Online]. Available: https://onlinelibrary.wiley.com/doi/abs/10.1002/adfm.201803020

[20] S. Lin, I. Akyildiz, P. Wang, and Z. Sun, "Distributed cross-layer protocol design for magnetic induction communication in wireless underground sensor networks," *IEEE Transactions on Wireless Communications*, vol. 14, no. 7, pp. 4006–4019, July 2015.

[21] N. Peplinski, F. Ulaby, and M. Dobson, "Dielectric properties of soil in the 0.3–1.3 ghz range," *IEEE Transactions on Geoscience and Remote Sensing*, vol. 33, no. 3, pp. 803–807, May 1995.

[22] M. A. Poletti, "The application of linearly swept frequency measurements," *The Journal of the Acoustical Society of America*, vol. 84, no. 2, pp. 599–610, August 1988.

[23] T. Rappaport, S. Seidel, and K. Takamizawa, "Statistical channel impulse response models for factory and open plan building radio communicate system design," *IEEE Transactions on Communications*, vol. 39, no. 5, pp. 794–807, May 1991.

[24] U. Raza and A. Salam, "On-site and external power transfer and energy harvesting in underground wireless," *Electronics*, vol. 9, no. 4, 2020.

[25] U. Raza and A. Salam, "Wireless underground communications in sewer and stormwater overflow monitoring: Radio waves through soil and asphalt medium," *Information*, vol. 11, no. 2, 2020.

[26] U. Raza and A. Salam, "Zenneck waves in decision agriculture: An empirical verification and application in em-based underground wireless power transfer," *Smart Cities*, vol. 3, no. 2, pp. 308–340, 2020. [Online]. Available: https://www.mdpi.com/2624-6511/3/2/17

[27] A. Salam, M. C. Vuran, and S. Irmak, "A statistical impulse response model based on empirical characterization of wireless underground channel," *IEEE Transactions on Wireless Communications*, 2020.

[28] A. Salam and M. C. Vuran, "Impacts of soil type and moisture on the capacity of multi-carrier modulation in internet of underground things," in *Proc. of the 25th ICCCN 2016*, Waikoloa, Hawaii, USA, Aug 2016.

[29] A. Salam and M. C. Vuran, "Impacts of soil type and moisture on the capacity of multi-carrier modulation in internet of underground things," in *Proc. of the 25th ICCCN 2016*, , Hawaii, USA, Aug 2016 (Best Student Paper Award).

[30] A. Salam and M. C. Vuran, "Smart underground antenna arrays: A soil moisture adaptive beamforming approach," Department of Computer Science and Engineering, University of Nebraska-Lincoln, Tech. Rep. TR-UNL-CSE-2017-0001, January 2017.

[31] A. Salam, "Pulses in the sand: Long range and high data rate communication techniques for next generation wireless underground networks," *ETD collection for University of Nebraska - Lincoln*, no. AAI10826112, 2018. [Online]. Available: http://digitalcommons.unl.edu/dissertations/AAI10826112

[32] A. Salam, "A comparison of path loss variations in soil using planar and dipole antennas," in *2019 IEEE International Symposium on Antennas and Propagation*.   IEEE, Jul 2019.

[33] A. Salam, "Design of subsurface phased array antennas for digital agriculture applications," in *Proc. 2019 IEEE International Symposium on Phased Array Systems and Technology (IEEE Array 2019)*, Waltham, MA, USA, Oct. 2019.

[34] A. Salam, "A path loss model for through the soil wireless communications in digital agriculture," in *2019 IEEE International Symposium on Antennas and Propagation*.   IEEE, Jul 2019.

[35] A. Salam, "Sensor-free underground soil sensing," in *ASA, CSSA and SSSA International Annual Meetings (2019)*.   ASA-CSSA-SSSA, 2019.

[36] A. Salam, "Subsurface mimo: A beamforming design in internet of underground things for digital agriculture applications," *Journal of Sensor and Actuator Networks*, vol. 8, no. 3, 2019. [Online]. Available: https://www.mdpi.com/2224-2708/8/3/41

[37] A. Salam, *Underground Environment Aware MIMO Design Using Transmit and Receive Beamforming in Internet of Underground Things*.   Cham: Springer International Publishing, 2019, pp. 1–15.

[38] A. Salam, "An underground radio wave propagation prediction model for digital agriculture," *Information*, vol. 10, no. 4, 2019. [Online]. Available: http://www.mdpi.com/2078-2489/10/4/147

[39] A. Salam, "Underground soil sensing using subsurface radio wave propagation," in *5th Global Workshop on Proximal Soil Sensing*, COLUMBIA, MO, May 2019.

[40] A. Salam, *Internet of Things for Environmental Sustainability and Climate Change*.   Cham: Springer International Publishing, 2020, pp. 33–69. [Online]. Available: https://doi.org/10.1007/978-3-030-35291-2_2

[41] A. Salam, *Internet of Things for Sustainability: Perspectives in Privacy, Cybersecurity, and Future Trends*.   Cham: Springer International Publishing, 2020, pp. 299–327. [Online]. Available: https://doi.org/10.1007/978-3-030-35291-2_10

[42] A. Salam, *Internet of Things for Sustainable Community Development*, 1st ed.   Springer Nature, 2020.

[43] A. Salam, *Internet of Things for Sustainable Community Development: Introduction and Overview*.   Cham: Springer International Publishing, 2020, pp. 1–31. [Online]. Available: https://doi.org/10.1007/978-3-030-35291-2_1

[44] A. Salam, *Internet of Things for Sustainable Forestry*.   Cham: Springer International Publishing, 2020, pp. 147–181. [Online]. Available: https://doi.org/10.1007/978-3-030-35291-2_5

[45] A. Salam, *Internet of Things for Sustainable Human Health*.   Cham: Springer International Publishing, 2020, pp. 217–242. [Online]. Available: https://doi.org/10.1007/978-3-030-35291-2_7

[46] A. Salam, *Internet of Things for Sustainable Mining*.   Cham: Springer International Publishing, 2020, pp. 243–271. [Online]. Available: https://doi.org/10.1007/978-3-030-35291-2_8

[47] A. Salam, *Internet of Things for Water Sustainability*.   Cham: Springer International Publishing, 2020, pp. 113–145. [Online]. Available: https://doi.org/10.1007/978-3-030-35291-2_4

[48] A. Salam, *Internet of Things in Agricultural Innovation and Security*.   Cham: Springer International Publishing, 2020, pp. 71–112. [Online]. Available: https://doi.org/10.1007/978-3-030-35291-2_3

[49] A. Salam, *Internet of Things in Sustainable Energy Systems*. Cham: Springer International Publishing, 2020, pp. 183–216. [Online]. Available: https://doi.org/10.1007/978-3-030-35291-2_6

[50] A. Salam, *Internet of Things in Water Management and Treatment*. Cham: Springer International Publishing, 2020, pp. 273–298. [Online]. Available: https://doi.org/10.1007/978-3-030-35291-2_9

[51] A. Salam, A. D. Hoang, A. Meghna, D. R. Martin, G. Guzman, Y. H. Yoon, J. Carlson, J. Kramer, K. Yansi, M. Kelly *et al.*, "The future of emerging iot paradigms: Architectures and technologies," 2019.

[52] A. Salam and U. Karabiyik, "A cooperative overlay approach at the physical layer of cognitive radio for digital agriculture," in *Third International Balkan Conference on Communications and Networking 2019 (BalkanCom'19)*, Skopje, Macedonia, the former Yugoslav Republic of, Jun. 2019.

[53] A. Salam and U. Raza, "On burial depth of underground antenna in soil horizons for decision agriculture," in *2020 International Conference on Internet of Things (ICIOT-2020)*, Honolulu, USA, Jun. 2020.

[54] A. Salam and S. Shah, "Internet of things in smart agriculture: Enabling technologies," in *2019 IEEE 5th World Forum on Internet of Things (WF-IoT) (WF-IoT 2019)*, Limerick, Ireland, Apr. 2019.

[55] A. Salam and M. C. Vuran, "EM-Based Wireless Underground Sensor Networks," in *Underground Sensing*, S. Pamukcu and L. Cheng, Eds. Academic Press, 2018, pp. 247 – 285.

[56] A. Salam, M. C. Vuran, X. Dong, C. Argyropoulos, and S. Irmak, "A theoretical model of underground dipole antennas for communications in internet of underground things," *IEEE Transactions on Antennas and Propagation*, 2019.

[57] A. Salam, M. C. Vuran, and S. Irmak, "Di-sense: In situ real-time permittivity estimation and soil moisture sensing using wireless underground communications," *Computer Networks*, vol. 151, pp. 31 – 41, 2019. [Online]. Available: http://www.sciencedirect.com/science/article/pii/S1389128618303141

[58] A. Salam and M. C. Vuran, "Smart underground antenna arrays: A soil moisture adaptive beamforming approach," in *Proc. IEEE INFOCOM 2017*, Atlanta, USA, May 2017.

[59] A. Salam and M. C. Vuran, "Smart underground antenna arrays: A soil moisture adaptive beamforming approach," in *Proc. IEEE INFOCOM 2017*, Atlanta, USA, May 2017.

[60] A. Salam and M. C. Vuran, "Wireless underground channel diversity reception with multiple antennas for internet of underground things," in *Proc. IEEE ICC 2017*, Paris, France, May 2017.

[61] A. Salam and M. C. Vuran, "Wireless underground channel diversity reception with multiple antennas for internet of underground things," in *Proc. IEEE ICC 2017*, Paris, France, May 2017.

[62] A. Salam, M. C. Vuran, and S. Irmak, "Pulses in the sand: Impulse response analysis of wireless underground channel," in *Proc. IEEE INFOCOM 2016*, San Francisco, USA, Apr. 2016.

[63] A. Salam, M. C. Vuran, and S. Irmak, "Pulses in the sand: Impulse response analysis of wireless underground channel," in *The 35th Annual IEEE International Conference on Computer Communications (INFOCOM 2016)*, San Francisco, USA, Apr. 2016.

[64] A. Salam, M. C. Vuran, and S. Irmak, "Towards internet of underground things in smart lighting: A statistical model of wireless underground channel," in *Proc. 14th IEEE International Conference on Networking, Sensing and Control (IEEE ICNSC)*, Calabria, Italy, May 2017.

[65] A. Salam, M. C. Vuran, and S. Irmak, "Towards internet of underground things in smart lighting: A statistical model of wireless underground channel," in *Proc. 14th IEEE International Conference on Networking, Sensing and Control (IEEE ICNSC)*, Calabria, Italy, May 2017.

[66] A. Saleh and R. Valenzuela, "A statistical model for indoor multipath propagation," *IEEE Journal on Selected Areas in Communications*, vol. 5, no. 2, pp. 128–137, February 1987.

[67] A. Street, L. Lukama, and D. Edwards, "Use of VNAs for wideband propagation measurements," *Communications, IEE Proceedings-*, vol. 148, no. 6, pp. 411–415, Dec 2001.

[68] Z. Sun and I. Akyildiz, "Channel modeling and analysis for wireless networks in underground mines and road tunnels," *IEEE Transactions on Communications*, vol. 58, no. 6, pp. 1758–1768, June 2010.

[69] X. Tan, Z. Sun, and I. F. Akyildiz, "Wireless underground sensor networks: Mi-based communication systems for underground applications." *IEEE Antennas and Propagation Magazine*, vol. 57, no. 4, pp. 74–87, Aug 2015.

[70] S. Temel, M. C. Vuran, M. M. Lunar, Z. Zhao, A. Salam, R. K. Faller, and C. Stolle, "Vehicle-to-barrier communication during real-world vehicle crash tests," *Computer Communications*, vol. 127, pp. 172 – 186, 2018. [Online]. Available: http://www.sciencedirect.com/science/article/pii/S0140366417305224

[71] M. J. Tiusanen, "Wideband antenna for underground Soil Scout transmission," *IEEE Antennas and Wireless Propagation Letters*, vol. 5, no. 1, pp. 517–519, December 2006.

[72] F. T. Ulaby and D. G. Long, *Microwave Radar and Radiometric Remote Sensing*. University of Michigan Press, 2014.

[73] M. C. Vuran and I. F. Akyildiz, "Channel model and analysis for wireless underground sensor networks in soil medium," *Physical Communication*, vol. 3, no. 4, pp. 245–254, December 2010.

[74] M. C. Vuran, A. Salam, R. Wong, and S. Irmak, "Internet of underground things in precision agriculture: Architecture and technology aspects," *Ad Hoc Networks*, 2018. [Online]. Available: http://www.sciencedirect.com/science/article/pii/S1570870518305067

[75] M. C. Vuran, A. Salam, R. Wong, and S. Irmak, "Internet of underground things: Sensing and communications on the field for precision agriculture," in *2018 IEEE 4th World Forum on Internet of Things (WF-IoT) (WF-IoT 2018)*, , Singapore, Feb. 2018.

[76] M. Win and R. Scholtz, "Characterization of ultra-wide bandwidth wireless indoor channels: a communication-theoretic view," *IEEE Journal on Selected Areas in Communications*, vol. 20, no. 9, pp. 1613–1627, Dec 2002.

Abdul Salam (S'04-M'18) (salama@purdue.edu) is an Assistant Professor with the Department of Computer and Information Technology, Purdue University, West Lafayette, IN, USA. His current research interests are in the areas of sustainability, wireless networking, digital agriculture, and Internet of Things. He was a Lecturer with the Department of Computer Science, Bahauddin Zakariya University, and the Department of Computer Science and Information Technology, Islamia University, Bahawalpur, Pakistan. He received the B.Sc. and M.S. degrees in computer science from Bahauddin Zakariya University, Multan, Pakistan, in 2001 and 2004, respectively, the M.S. degree in computer engineering from UET, Taxila, Pakistan, in 2012, and the Ph.D. degree in computer engineering from the Department of Computer Science and Engineering, University of Nebraska–Lincoln, Lincoln, NE, USA. He is among the top 10 highly cited researchers in the field of digital agriculture. Abdul Salam is the author of the book Internet of Things for Sustainable Community Development.

Mehmet C. Vuran (S'98-M07) (mcvuran@cse.unl.edu) received his B.Sc. degree in Electrical and Electronics Engineering from Bilkent University, Ankara, Turkey, in 2002. He received his M.S. and Ph.D. degrees in Electrical and Computer Engineering from the Georgia Institute of Technology, Atlanta, in 2004 and 2007, respectively, under the guidance of Prof. Ian F. Akyildiz. Currently, he is the Susan J. Rosowski Associate Professor of Computer Science and Engineering at the University of Nebraska-Lincoln and Robert B. Daugherty Water for Food Institute Fellow. He was recognized as the Thomson Reuters/Clarivate Analytics Highly Cited Researcher in computer science in 2014, 2015, and 2016. He is the recipient of an NSF CAREER award in 2010 and the co-author of Wireless Sensor Networks textbook. His current research interests include wireless underground communications, cognitive radio networks, cross-layer design, and correlation-based communication. He is an Associate Editor of IEEE Communications Surveys and Tutorials, Computer Networks Journal (Elsevier), and IEEE Transactions on Network Science and Engineering

Suat Irmak is a Harold W. Eberhard Distinguished Professor in the Department of Biological Systems Engineering at the University of Nebraska-Lincoln. In addition, he has Courtesy Full Professor appointments in the Departments of Earth and Atmospheric Sciences and Agronomy and Horticulture. He has a doctorate degree in agricultural and biological engineering with the emphasis on land and soil-water resources and irrigation engineering from the University of Florida. He holds numerous leadership roles in the American Society of Civil Engineers-Environmental and Water Resources Institute, for which he chairs the Evapotranspiration in Irrigation Hydrology Committee; American Society of Agricultural and Biological Engineers (ASABE); United States Committee on Irrigation and Drainage; and others. He has earned numerous awards and honors, including the ASABE John Deere Gold Medal Award, Heermann Sprinkler Irrigation Award, New Holland Young Researcher Award and the ASABE Young Extension Professional Award. Suat Irmak's research, extension and educational programs apply engineering and scientific fundamentals in soil and water resources engineering, irrigation engineering and agricultural water management, crop water productivity, evapotranspiration and other surface energy fluxes for agro-ecosystems; invasive plant species water use; and impacts of changes in climate variables on water resources and agro-ecosystem productivity. Irmak leads the Nebraska Agricultural Water Management Network, which aims to increase adoption of new tools, technologies (including advanced soil moisture sensing devices) and strategies for increasing crop water productivity and reducing energy use in agriculture. He established the Nebraska Water and Energy Flux Measurement, Modeling and Research Network, made up of 12 water and surface energy flux towers forming a comprehensive network that measures surface energy and water vapor fluxes, microclimatic variables, plant physiological parameters and biophysical properties, water use efficiency, soil water content, surface characteristics and their interactions for various agro-ecosystems.